Synthesis and characterization of compounds $Sr_2RMCu_2O_{8-\delta}$ (R = Pr, Nd, Sm, Eu, Gd; M = Nb, Ta)

M. Vybornov
Institut für Physikalische Chemie, Universität Wien, Währingerstrasse 42, A-1090 Wien, Austria

W. Perthold, H. Michor, T. Holubar, and G. Hilscher
Institut für Experimentalphysik, T.U.Wien, Wiedner Hauptstraße 8-10, A-1040 Wien, Austria

P. Rogl
Institut für Physikalische Chemie, Universität Wien, Währingerstrasse 42, A-1090 Wien, Austria

P. Fischer
Laboratorium für Neutronenstreuung, ETH Zürich und Paul Scherrer Institut, CH-5232, Villigen PSI, Switzerland

M. Divis
Department of Metal Physics, Charles University, CZ 121 16 Praha 2, Czech Republic
(Received 24 January 1995; revised manuscript received 15 March 1995)

The compounds $Sr_2RMCu_2O_{8-\delta}$ with R = Pr, Nd, Sm, Eu, Gd and M = Nb, Ta have been synthesized and characterized. Rietveld structure refinements reveal that the title compounds crystallize in the so-called "2112" structural type of $Ba_2LaMCu_2O_{8-\delta}$ (M = Nb,Ta). With respect to the different crystal symmetries reported earlier for $Ba_2LaNbCu_2O_{8-\delta}$, x-ray refinements of the crystal structure for all the compounds were performed in comparison for the two crystal symmetries: $P4/mmm$ and $I4/mcm$. Neutron powder diffraction data for $Sr_2PrTaCu_2O_{8-\delta}$ confirmed the body centered tetragonal symmetry. An internally consistent set of the structural parameters is obtained for the whole series of the title compounds. Magnetic ordering of the Cu sublattice, as monitored on the $(103)^m$ reflection was observed below 190 K for $Sr_2PrTaCu_2O_{8-\delta}$. Although traces of superconductivity (< 0.2%) have been detected in $Ba_2LaM_{1-x}W_xCu_2O_{8-\delta}$ ($x \sim 0.3, M$ =Nb,Ta) below 30 K, the superconducting impurity phase could not be resolved. The antiferromagnetic (AF) order of the rare-earth sublattice in this R-2112 system (e.g., $T_N^{Gd} = 2.18$ K) appears to be similar to that of the $RBa_2Cu_3O_{7-\delta}$ series (e.g., $T_N^{Gd} = 2.29$ K); however, the exceptional high AF order of Pr in Pr-123 (with 17 K) is reduced to below 2.3 K for $Sr_2PrMCu_2O_{8-\delta}$. The temperature and field dependence of the specific heat and the susceptibility is discussed in terms of crystal field splitting derived from the $RBa_2Cu_3O_{7-\delta}$ compounds. Overall crystal field splitting in the title compounds is comparable with that of the R-123 compounds.

I. INTRODUCTION

Compounds derived from the $YBa_2Cu_3O_7$ ("123") structural type include the recent discovery of the so-called "2112" family of layered copper oxides in the systems $Ba_2LaNbCu_2O_8$ (Refs. 1–3) and $Ba_2RMCu_2O_8$, with R = Pr, Nd and M = Nb or Ta.[4] Despite the fact that the 2112 phase has the same metal stoichiometry as the 123 superconducting system the 2112 phase is interestingly lacking superconductivity. For the 2112 compounds the CuO chains of the 123 system are replaced by layers of NbO_2 (TaO_2), as the result of a complete substitution of Cu atoms by Nb (Ta) atoms. The stabilization of the carrier source to the CuO layers, as the preliminary goal of the replacement Nb (Ta) for Cu, resulted, however, in a comparatively high stability of the oxygen sites in the NbO_2 (TaO_2) planes. This fact does not allow sufficient doping of the 2112 phase to establish superconductivity, although band structure calculations suggested that superconductivity in the 2112 compounds may be induced by proper chemical substitutions.[5]

Two different crystal symmetries have been reported for the homologous 2112 compound $Ba_2LaNbCu_2O_8$. Whereas the space group $P4/mmm$ was used by Greaves and Slater[3] to describe the structure of this compound on the basis of x-ray diffraction data, a neutron diffraction analysis by Rey *et al.*[2] revealed a higher crystal symmetry $I4/mcm$.

Table I gives an overview of the existing known 2112 phases. Attempts to synthesize the 2112 Ba-based phase for R = Sm, Eu, Gd, and Y were not successful. The reason for this was claimed[3] to be a size effect, with Y and rare-earth ions smaller than Nd being unable to form the 2112 phase; their samples merely resulted in a mixture of perovskite Ba_2RMO_6, CuO, and another unidentified impurity phase. The rare-earth cation in Ba_2RMO_6 occupies the small octahedral site, which for smaller rare earths makes the formation of this perovskite more probable than the 2112 phase. However, the Sr-

TABLE I. Ionic size effect in the formation of Ba- and Sr-based 2112 phases $A_2RMCu_2O_{8-\delta}$ (A = Ba, Sr; R =La, Pr, Nd, Sm, Eu, Gd, Y; M =Nb, Ta). Y, phase exists; N, no phase formed. Data from Refs. 1–4, 6, 7 and present work.

R	La	Pr	Nd	Sm	Eu	Gd	Y
R^{3+} (CN = 8)[a], ionic radius, nm	0.1160	0.1126	0.1109	0.1079	0.1066	0.1053	0.1019
A = Ba, M = Nb	Y	Y	Y	N	N	N	N
A = Ba, M = Ta	Y	Y	N	N	N	N	N
A = Sr, M = Nb	N	Y	Y	Y	Y	Y	N
A = Sr, M = Ta	N	Y	Y	Y	Y	Y	N

[a]Reference 8.

based 2112 phase was successfully synthesized for a much wider range of rare earths: R = Pr and Sm by Hellebrand *et al.*[6] and for R = Nd–Gd by Brnicevic *et al.*[7] In both publications lattice parameters were reported for the $P4/mmm$ symmetry.

With respect to local structural changes the rare-earth substitution in $Sr_2RMCu_2O_{8-\delta}$ provides an alternative method to study compounds derived from the $YBa_2Cu_3O_7$ structural type in comparison to our previously reported studies on $(Ba_{1-x}Sr_x)_2PrNbCu_2O_{8-\delta}$.[9] There isoelectronic Ba/Sr substitution was found to produce an anomalous expansion of the average Pr-oxygen bond and was accompanied by the reduction of the antiferromagnetic ordering temperature T_N of the Pr sublattice. Due to the fact that rare-earth ions are situated between CuO_2 planes, a change of the rare-earth ion in $Sr_2RMCu_2O_{8-\delta}$ mostly affects the nearest neighboring Cu and O(2) ions, but leaves the Sr, M, O(1), and O(4) ions nearly untouched, whereas in $(Ba_{1-x}Sr_x)_2PrNbCu_2O_{8-\delta}$ changes are caused by Ba/Sr replacement on the site between CuO_2 planes and NbO_6 octahedra.

The aim of the present work is the crystallographic analysis and the characterization of the physical properties of the novel compounds $Sr_2RMCu_2O_{8-\delta}$ for the series of the rare earths from Pr to Gd and for M= Nb and Ta.

II. EXPERIMENTAL DETAILS

A series of ceramic samples with the general formula $Sr_2RMCu_2O_{8-\delta}$ with R = Pr, Nd, Sm, Eu, Gd

TABLE II. Experimental neutron diffraction data for $Sr_2PrTaCu_2O_8$.

Sample container	Vanadium cylinder, R = 7.5 mm
Temperature [K]	10–296
Neutron wavelengths [nm]	0.16984 (h. resol.), 0.17031 (h. intensity)
Absorption correction	μR = 0.1440
Reactor	Saphir, PSI CH-Villigen
Monochromator	Germanium (311) (h. resol. mode)
Soller slits	10′/-/12′
2Θ range [2Θ]	3.0–134.9
Step scan increment [2Θ]	0.1
Coherent scattering lengths [fm]	Sr 7.02
	Pr 4.58
	Ta 6.91
	Cu 7.718
	O 5.803
Number of contributing reflections	145
Background	Background refinement (six parameters)
Preferred orientation	[001]
Number of variables	30
Secondary impurity phase	$Sr_3Cu_2TaO_9$
Largest element of correlation matrix	0.7
Maximal Δ/σ	< 0.01

Residual values:

$$R_I = \sum |I_i(\text{obs}) - (1/c)I_i(\text{calc})| / \sum I_i(\text{obs})$$

$$R_F = \sum |[I_i(\text{obs})]^{1/2} - (1/c)[I_i(\text{calc})]^{1/2}| / \sum [I_i(\text{obs})]^{1/2}$$

$$R_P = \sum |Y_i(\text{obs}) - (1/c)Y_i(\text{calc})| / \sum Y_i(\text{obs})$$

$$R_{wP} = [\sum w_i |Y_i(\text{obs}) - (1/c)Y_i(\text{calc})|^2 / \sum w_i |Y_i(\text{obs})|^2]^{1/2}$$

$$R_e = \{(N - P + C) / \sum w_i Y_i(\text{obs})\}^{1/2}$$

$$\chi^2 = \{R_{wP}/R_e\}$$

I_i Integrated intensity of reflection i
w_i Weighting function
Y_i Number of counts (background corrected) at 2Θ
c Scale factor
N Number of points in the pattern
P Number of refined parameters
C Number of constraint functions

and M = Nb, Ta each with a total mass of 0.5–2.5 g, was synthesized by reaction sintering. Powders of Nb_2O_5 ("Schuchardt"),Ta_2O_5 ("Aldrich"), Pr_6O_{11}, Nd_2O_3, Sm_2O_3, Eu_2O_3, Gd_2O_3 ("Auer Remy"), $SrCO_3$ ("Ventron"), and CuO ("Merck"), each with a minimum purity of 99.9%, were used as starting materials. Rare-earth oxides were calcined in air prior to use at 900 °C. Stoichiometric amounts of starting materials were mixed in an agate mortar and pressed into pellets prior to repeated annealing (2–3 times) with intermediate steps of grinding and recompacting. The samples were annealed in air at 1000 °C for 18 h and then quenched to room temperature.

Precise lattice parameters were determined at room temperature by means of x-ray powder diffraction (XRD) with monochromatized Cu Kα radiation (λ = 0.154 056 nm) in a Guinier-Huber camera (R = 114.59 mm) employing an internal standard of 99.9999% pure Ge (a_{Ge} = 0.565 790 6 nm). XRD intensity data for powder structure refinement were obtained from flat samples in a Siemens D5000 diffractometer with Cu Kα radiation. The diffractometer was operated in the step scan mode with $5° \leq 2\theta \leq 120°$, $\Delta\theta = 0.01°$, and a step time of 60–100 sec. Rietveld full matrix full profile refinements were performed using the program DBW.[10]

A large sample specimen of $Sr_2PrTaCu_2O_8$ ($\simeq$ 20 g) also was prepared for a neutron diffraction experiment employing the multidetector powder diffractometer DMC at the 10 MW Saphir reactor in Villingen (PSI), Switzerland, with neutron wavelength λ = 0.169 48 nm (high resolution mode) or λ = 0.170 31 nm (high intensity mode) and resolution $\Delta d/d \geq 4 \times 10^{-3}$ (see Ref. 11). Preferred orientation effects were minimized by powdering the sample to a grain size smaller than 25 μm and by sample oscillation during the measurements. Further details concerning the experiment are summarized in Table II including the definition for a series of reliability measures. Atom distribution, precise atom parameters and occupancies, individual thermal factors, and profile parameters were derived from a least squares powder profile refinement[10] using the neutron scattering lengths of Sears.[12]

Specific heat measurements were performed in an automatic calorimeter in external fields up to 11 T using the step heating technique. Susceptibility and magnetization measurements were carried out in a calibrated ac susceptometer in the frequency range from 10 Hz to 1 kHz with a field amplitude of 0.1 mT and in a 6-T superconducting quantum interference device (SQUID) magnetometer, respectively.

III. RESULTS AND DISCUSSION

A. Crystallographic characterization

1. *Neutron diffraction of $Sr_2PrTaCu_2O_{8-\delta}$*

Refinements of the neutron diffraction data at 295 K and 9 K based on the simple structure model in $P4/mmm$ were not better than $R_F \simeq 0.11$. A significant decrease of the residual value to $R_F \leq 0.048$ can be achieved transferring the structure model to the $I4/mcm$ supergroup according to a simple crystallographic supergroup-group relationship $I4/mcm \rightarrow k_2(a_0/\sqrt{2}, c_0/2) \rightarrow P4/mmm$, thereby releasing a series of structural constraints, particularly of the oxygen atoms. In the course of the refinement small amounts of a cubic perovskite-type phase Sr(Ta,Cu)O_3 became obvious, which was simultaneously refined as a secondary phase. The final structural and profile parameters as well as agreement indices are given in Table III including metal-oxygen bond distances for the refinement of the 9 K pattern. As seen from the residual values in Table III observed and calculated neutron intensities are in excellent agreement. Freeing the occupancies of all metal atoms did not reveal any significant deviations from full atom occupation. Determination of metal occupancies is of higher significance in the corresponding x-ray refinement, due to the higher x-ray scattering power of the metal atoms as compared to the neutron case (see below).

The crystal structure of $Sr_2PrTaCu_2O_{8-\delta}$ is presented in Fig. 1, revealing a three-dimensional perspective of the CuO_2 planes and TaO_6 octahedra. Figure 2 shows an overview along [001] on the tilting of the corner connected TaO_6 octahedra. It is clearly displayed for the upmost

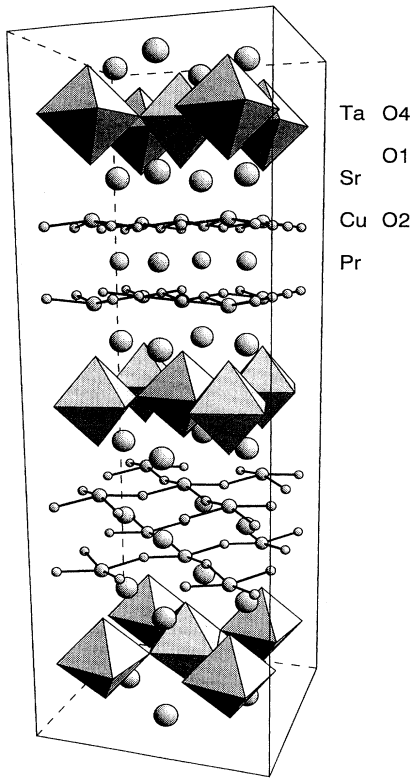

FIG. 1. Crystal structure of $Sr_2PrTaCu_2O_{8-\delta}$ in a three-dimensional perspective view of the CuO_2 planes and TaO_6 octahedra.

Cu-O(2) layer in Fig. 1 that all of the oxygen ions O(2) lie in the same plane. As documented in Table III there is only a small change in the tilting angle of the TaO_6 octahedra $Ta[O(1)_2,O(4)_4]$ between 9 K and 295 K. In contrast to the x-ray evaluation (see below) which is less sensitive to oxygen movements, there is no variation in x and y for the O(2) atom out of its pseudospecial position in the 16*l* site (1/4, 3/4, 0.1835). Whereas the series of measurements at temperatures between 9 K and 295 K proved that the z parameters of the atoms are practically insensitive to temperature, the tilting of the octahedra as monitored via the x, y parameters of the O(4) atom shows a slight temperature dependence. TaO_6 tilting angles are in reasonably good accordance with the results obtained from x-ray data (see below).

The temperature dependence of both lattice parameters in the region from 9 to 295 K is shown in Fig. 3, revealing the usual monotonic increase.

Difference diffraction spectra between room-temperature and low-temperature runs revealed only one significant peak of magnetic origin at $2\theta = 21.8°$, which perfectly corresponds to the (103) reflection extinct in

TABLE III. Crystallographic data for $Sr_2PrTaCu_2O_8$ ($Ba_2LaNbCu_2O_8$ type). Neutron diffraction data. Temperature factor $T = \exp[-B(\sin\Theta/\lambda)^2]$, standard deviations are in parentheses. Space group I/4*mcm* (No. 140), origin at center, $Z = 4$.

Neutron powder diffraction at 295 K, λ = 0.16984 nm.

a = 0.55033(4), c = 2.3445(2) nm, c/a = 4.260, V = 0.7101 nm^3.

Atom	Site	x	y	z	B, 10^2 nm^2	Occupancy
Sr	8g	0.0	0.5	0.0987(2)	1.2(1)	1.0
Pr	4b	0.0	0.5	0.25	0.3(2)	1.0
Ta	4c	0.0	0.0	0.0	0.4(1)	1.0
Cu	8f	0.0	0.0	0.1756(1)	0.3(1)	1.0
O(1)	8f	0.0	0.0	0.0830(3)	2.0(2)	1.0
O(4)	8h	0.1967(15)	0.6967(15)	0.0	2.0(2)	0.92(2)
O(2)	16l	0.2500(7)	0.7500(7)	0.1788(19)	0.7(1)	1.0

$R_p = 0.049$ $R_{wp} = 0.070$ $R_F = 0.048$.

Neutron powder diffraction at 9 K, λ = 0.17031 nm.

a = 0.54906(3), c = 2.3374(2) nm, c/a = 4.257, V = 0.7046 nm^3.

Atom	Site	x	y	z	B, 10^2 nm^2	Occupancy
Sr	8g	0.0	0.5	0.0989(1)	0.4(1)	1.0
Pr	4b	0.0	0.5	0.25	0.2(1)	1.0
Ta	4c	0.0	0.0	0.0	0.1(1)	1.0
Cu	8f	0.0	0.0	0.1758(1)	0.1(1)	1.0
O(1)	8f	0.0	0.0	0.0832(2)	1.2(1)	1.0
O(4)	8h	0.1896(10)	0.6896(10)	0.0	1.2(2)	0.92(2)
O(2)	16l	0.2500(5)	0.7500(5)	0.1834(2)	0.3(1)	1.0

$R_p = 0.044$ $R_{wp} = 0.064$ $R_F = 0.033$.

Bond distances within first nearest neighbor coordination, nm:

Sr - 4 O(1)	0.2769	Pr - 4 O(2)	0.2488	Ta - 2 O(1)	0.1944	Cu - 1O(1)	0.2164
- 2 O(4)	0.2740	- 4 O(2)	0.2488	- 4 O(4)	0.1997	- 4 O(2)	0.1949
- 2 O(4)	0.3339						
- 2 O(2)	0.2769						
- 2 O(2)	0.2769						

Temperature, K	295	9
"Puckering angle" Cu-O(2)-Cu	169.1	169.5
Tilting angle of $Ta[O(1)_2,O(4)_4]$ octahedra	12.0	13.6

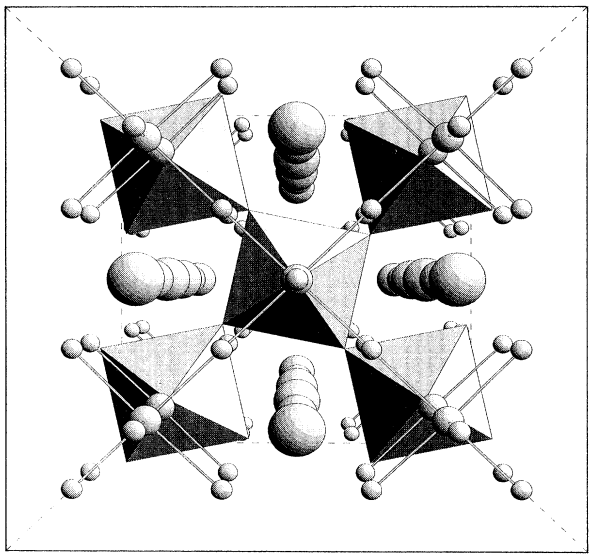

FIG. 2. A view along [001] on the tilting of the corner connected TaO_6 octahedra in $Sr_2PrTaCu_2O_{8-\delta}$.

the nuclear cell with symmetry $I4/mcm$. Figure 4 shows the temperature dependence of the integrated intensity of the (103) reflection which goes to zero at ~190 K. The weak intensity of the magnetic reflection indicates a saturation moment of $\sim 0.3\mu_B$ or less, probably to be attributed to weak magnetic interactions within the Cu sublattice. The type of ordering, however, seems to be different from isotypic $Ba_2PrNbCu_2O_8$ where the prominent magnetic peak corresponds to the (102) reflection and vanishes at $T_N = 340$ K.[13]

2. *X-ray diffraction*

Two different crystal symmetries were earlier reported for the parent 2112 compound $Ba_2LaNbCu_2O_{8-\delta}$ (Ref. 2) and for $Ba_2RNbCu_2O_{8-\delta}$ (R= Pr, Nd).[13] We have performed the x-ray refinements of the crystal structure for all $Sr_2RMCu_2O_{8-\delta}$ compounds for both crystal symmetries $P4/mmm$ and $I4/mcm$, but since the neutron powder diffraction data clearly confirmed the $I4/mcm$ symmetry, the analysis of the x-ray diffraction data is only reported for the latter model.

Guinier photographs and powder x-ray diffractograms for all samples $Sr_2RMCu_2O_{8-\delta}$ were indexed completely on the basis of a tetragonal-body-centered unit cell and revealed close resemblance to the structure of $Ba_2LaNbCu_2O_{8-\delta}$.

Results of our previous investigation on $(Ba,Sr)_2PrNbCu_2O_8$ (see Ref. 9) confirmed a significant improvement of the phase purity of the samples with off-

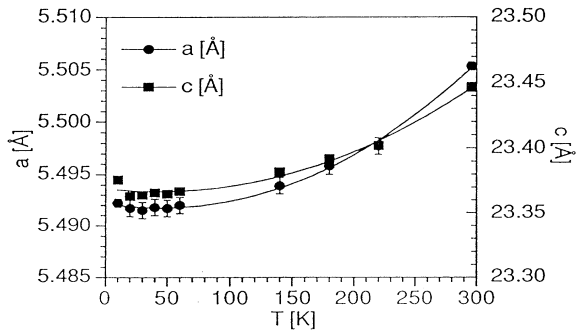

FIG. 3. Variation of lattice parameters vs temperature for $Sr_2PrTaCu_2O_{8-\delta}$ from neutron diffraction.

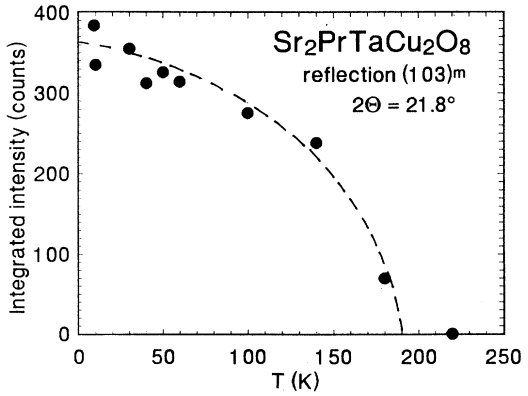

FIG. 4. Temperature dependence of the integrated intensity of the (103) magnetic neutron reflection in $Sr_2PrTaCu_2O_8$.

stoichiometric compositions $Ba_{2-x}R_{1+x}M_{1-x}Cu_{2+x}O_8$ for $x = 0.1$, R = La, Pr, and M = Nb, Ta, as was previously reported by Greaves and Slater,[3] and by Jhans *et al.*[14] for $Sr_2RNbCu_2O_8$. For Sr-2112 systems, however, neither the ratio between the main and secondary (impurity) phases nor the physical properties of our samples could be improved for the off-stoichiometric compositions $Sr_{2-x}R_{1+x}M_{1-x}Cu_{2+x}O_8$ when x was $x = 0.1$, 0.2, or 0.3, R = Pr, Gd, and M = Nb, Ta. Moreover, the qualitative analysis for R = Gd of both Nb- and Ta-based samples shows an even larger amount of secondary phase(s) for the off-stoichiometric samples than for stoichiometric ones. Therefore this report exclusively deals with the results obtained on stoichiometric samples $Sr_2RMCu_2O_{8-\delta}$ for the whole range of combinations studied.

Table IV summarizes the results of our refinements. Rietveld full matrix full profile refinements were carried out in the following sequence. First, the background, cell parameters, atomic coordinates, and equivalent ther-

TABLE IV. Structural parameters and selected bond distances for $Sr_2RMCu_2O_{8-\delta}$ determined from Rietveld refinement. XRD data obtained at room temperature on a Siemens D5000 powder diffractometer B in 10^2 nm^2. Standard deviations in parentheses. Details of agreement factors are given in Table II. Space group $I4/mcm$ (No. 140) origin at center, $Z = 4$.

R	Pr		Nd		Sm		Eu		Gd	
radius for R^{3+}, nm	0.1126		0.1109		0.1079		0.1066		0.1053	
M	Nb	Ta	Nb	Ta	Nb	Ta	Nb	Ta	Nb	Ta
a, nm	0.550666(9)	0.550186(8)	0.55037(1)	0.549376(8)	0.548422(5)	0.547938(8)	0.54788(1)	0.547377(9)	0.54744(1)	0.547099(8)
c, nm	2.33642(8)	2.3446(6)	2.33565(8)	2.34179(6)	2.32887(4)	2.33671(6)	2.3274(1)	2.33357(6)	2.32597(9)	2.33195(5)
8Sr in 8g (1/2,0,z)										
z	0.0984(1)	0.0980(1)	0.0986(1)	0.0986(1)	0.0989(1)	0.0992(1)	0.0993(1)	0.0996(1)	0.0998(1)	0.1008(2)
B	0.3(1)	0.78(8)	1.3(1)	0.80(9)	0.54(8)	0.93(7)	0.56(3)	0.41(9)	1.0(1)	0.57(3)
4R in 4b (1/2,0,1/4)										
B	0.29(1)	0.48(9)	0.60(9)	0.34(4)	0.32(6)	0.6(1)	0.3(1)	0.3(1)	0.16(1)	0.27(1)
n	0.99(1)	0.94(5)	0.96(1)	0.95(2)	1.0	0.96(1)	1.0	0.95(1)	0.96(1)	0.99(1)
4M in 4c (0,0,0)										
B	0.66(9)	0.67(5)	1.8(1)	0.63(7)	0.9(1)	0.6(1)	0.79(1)	0.84(6)	0.55(1)	0.09(4)
n	0.96(1)	0.92(5)	1.00(1)	0.94(3)	1.01(1)	0.94(1)	1.02(1)	0.97(1)	1.00(1)	0.97(1)
8Cu in 8f (0,0,z)										
z	0.1749(3)	0.1756(2)	0.1758(3)	0.1763(2)	0.1777(2)	0.1769(2)	0.1770(3)	0.1779(2)	0.1778(3)	0.1788(2)
B	0.19(2)	0.95(4)	0.6(1)	0.78(7)	0.20(6)	0.99(7)	0.29(2)	0.85(2)	0.25(1)	0.10(1)
8O1 in 8f (0,0,z)										
z	0.083(1)	0.0821(7)	0.075(1)	0.0814(7)	0.0784(8)	0.0809(7)	0.0829(9)	0.0821(7)	0.0798(9)	0.0810(9)
B	0.25(6)	2.5(5)	2.6(7)	1.8(7)	1.8(5)	1.3(7)	0.3(1)	0.5(1)	1.4(7)	0.93(6)
n	0.91(3)	1.0	1.0	1.01(4)	1.0	1.04(3)	1.0	1.04(3)	1.0	1.0
8O4in 8h (x,1/2+x,0)										
x	0.312(3)	0.315(3)	0.328(4)	0.272(2)	0.319(2)	0.275(2)	0.312(3)	0.281(3)	0.314(4)	0.316(4)
B	0.7(5)	2.7(9)	2.9(9)	1.02(5)	0.8(5)	0.82(6)	2.9(6)	0.72(9)	1.3(8)	2.7(9)
n	1.0	0.98(3)	1.0	1.00(3)	1.0	1.04(5)	1.0	1.0	1.0	1.0
16O2 16l (x,1/2+x,z)										
x	0.248(5)	0.240(5)	0.241(5)	0.235(5)	0.238(3)	0.244(7)	0.234(5)	0.250(7)	0.238(5)	0.244(9)
z	0.1796(8)	0.1849(4)	0.1795(8)	0.1856(4)	0.1820(5)	0.1870(4)	0.1806(8)	0.1893(5)	0.1839(8)	0.1880(6)
B	1.5(3)	1.6(3)	2.4(4)	0.30(5)	0.9(3)	1.1(5)	2.8(5)	0.91(6)	1.1(4)	0.3(4)
n	1.0	1.0	1.0	1.0(1)	1.0	1.05(3)	1.0	1.02(3)	1.0	1.0
R_{wp}	0.049	0.039	0.051	0.038	0.027	0.035	0.041	0.033	0.034	0.042
R_I	0.054	0.042	0.066	0.042	0.042	0.047	0.061	0.048	0.060	0.058
R_F	0.046	0.058	0.071	0.053	0.060	0.065	0.079	0.058	0.086	0.066
χ^2	1.40	1.25	1.54	1.33	1.11	1.24	1.63	1.26	1.32	1.31

R	Pr		Nd		Sm		Eu		Gd	
M	Nb	Ta	Nb	Ta	Nb	Ta	Nb	Ta	Nb	Ta
Sr - 4 O1	0.2777	0.2776	0.2807	0.2776	0.2783	0.2773	0.2766	0.2767	0.2776	0.2774
2 O4	0.2726	0.2711	0.2664	0.2910	0.2697	0.2901	0.2732	0.2877	0.2732	0.2748
2 O4	0.3345	0.3360	0.3438	0.3130	0.3380	0.3149	0.3344	0.3183	0.3361	0.3392
2 O2	0.2707	0.2764	0.2663	0.2736	0.2674	0.2790	0.2621	0.2851	0.2687	0.2775
2 O2	0.2730	0.2871	0.2763	0.2897	0.2806	0.2854	0.2798	0.2851	0.2818	0.2839
RE - 4 O2	0.2537	0.2412	0.2496	0.2368	0.2432	0.2396	0.2428	0.2398	0.2400	0.2378
4 O2	0.2561	0.2534	0.2603	0.2552	0.2576	0.2470	0.2619	0.2398	0.2545	0.2452
M - 2 O1	0.1939	0.1925	0.1752	0.1906	0.1826	0.1890	0.1929	0.1916	0.1856	0.1889
4 O4	0.2006	0.2010	0.2038	0.1950	0.2011	0.1947	0.1996	0.1950	0.1998	0.2001
Cu - 1 O1	0.2147	0.2192	0.2354	0.2222	0.2313	0.2243	0.2190	0.2236	0.2279	0.2281
4 O2	0.1950	0.1959	0.1949	0.1958	0.1944	0.1952	0.1943	0.1953	0.1943	0.1947
1 Cu	0.3509	0.3489	0.3466	0.3452	0.3368	0.3416	0.3398	0.3365	0.3359	0.3321
"Puckering angle" Cu-O2-Cu	173.5	167.2	174.5	167.2	174.1	166.0	175.1	164.4	171.6	167.3
Tilting angle of $Cu[O1,O2_4]$ pyramid	0.5	2.3	2.0	3.4	2.7	1.4	3.7	0.0	2.7	1.4
Tilting angle of $M[O1_2,O4_4]$ octahedra	13.9	14.6	17.3	5.0	15.4	5.7	13.9	7.1	14.4	14.8

mal parameters were refined. Then, the occupancies of the atom sites were allowed to vary one after another, starting with the heaviest atom down to the light oxygen atoms. In the case of divergence or inconsistency of the refinement, the occupancy of the particular atom site was fixed to its theoretical value and the refinement was repeated. In this manner it was possible to refine the occupancies of the rare-earth and Nb/Ta atom sites for all compounds studied and in some cases also oxygen site occupancies. Occupancy of Sr was fixed at its theoretical value. A cubic perovskite phase $Sr(M,Cu)O_3$ was found in small amounts for R = Pr, Nd for M = Nb and R = Pr, Gd for M = Ta and was refined simultaneously as a secondary phase. As an example the typical best fit of the refinement for $Sr_2SmNbCu_2O_{8-\delta}$ is shown in Fig. 5.

As found earlier by Rey *et al.*[2] for $Ba_2LaNbCu_2O_8$, both crystal structural models seem to fit the x-ray diffraction pattern quite well, with the positional parameters similar for all atoms, except those for the O(4) atom. This atom appears significantly displaced from its ideal site at (1/4, 3/4, 0) in a direction perpendicular to the bond Nb-O(4), indicating a rotation of the NbO_6 octahedra around the [001] axis. Critical analyses of our refinements give similar results for the series $Sr_2RMCu_2O_{8-\delta}$, except that displacements are observed for both the O(4) and O(2) atom sites. The one for O(4) is much larger, up to (0.328, 0.828, 0) for $Sr_2NdNbCu_2O_{8-\delta}$, which means a much larger tilting angle of the $Nb[O(1)_2,O(4)_4]$ octahedra of about 17°. The O(2) displacement in (001) from its ideal position (1/4, 3/4, z) varies as a function of the rare earth for Nb-based samples: It is almost negligible for Pr (0.248, 0.748, 0.1796) whereas it reaches a value of (0.234, 0.734, 0.1806) for Eu, indicating an increase of the tilting angle of the $Cu[O(1),O(2)_4]$ pyramid from 0.5° to 3.7° for $Sr_2PrNbCu_2O_{8-\delta}$ and $Sr_2EuNbCu_2O_{8-\delta}$, respectively. For the Ta-based system the corresponding angle varies from 0.0° to 4.3° for $Sr_2EuTaCu_2O_{8-\delta}$ and $Sr_2NdTaCu_2O_{8-\delta}$, respectively.

Considering the generally small contributions of the oxygen atoms to the overall x-ray structure factors, the residual values offer no decisive preference for the "correct" structure model. Temperature factors B, however, reveal a clear improvement for the atom arrangement in the body-centered symmetry $I4/mcm$, where oxygen atoms show relief from the unbalanced temperature movements in $P4/mmm$.

Results of the lattice parameter refinements as a function of the rare-earth ionic radius for the series $Sr_2RMCu_2O_{8-\delta}$ are presented in Fig. 6 on the basis of the $I4/mcm$ unit cell. Open symbols represent data obtained from Guinier photographs, while solid symbols are from Rietveld refinements of diffractometer data. The lattice parameters vary almost linearly within the series of the rare earths from Pr to Gd, according to the lanthanide contraction, and the values obtained by both techniques are in fine agreement.

Whereas parameter a shrinks by 5.9% for the Nb sys-

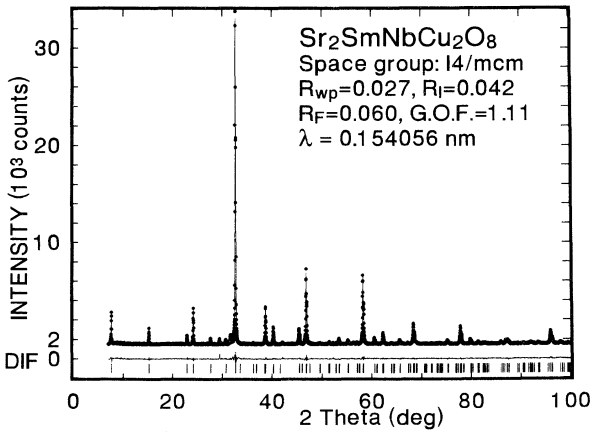

FIG. 5. Typical Rietveld refinement plot for $Sr_2SmNbCu_2O_{8-\delta}$ for the body-centered symmetry $I4/mcm$. Measured XRD data are represented by dots, calculated profile and difference are shown as solid lines, and the location of the Bragg reflections is marked underneath by vertical bars.

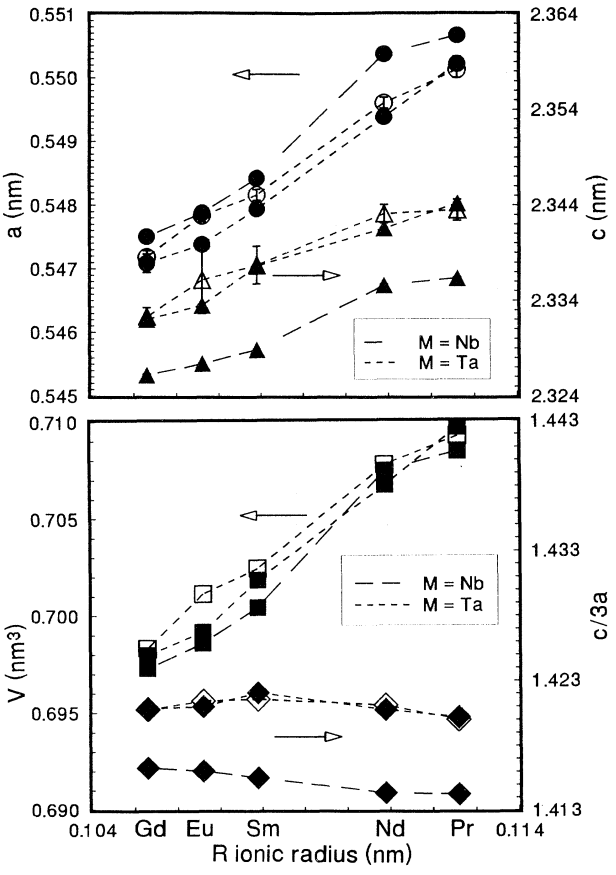

FIG. 6. Lattice parameters a and c, unit cell volume V, and $c/3a$ ratio vs rare-earth ionic radius for $Sr_2RMCu_2O_{8-\delta}$ (R = Pr, Nd, Sm, Eu, Gd, and M = Nb, Ta). Open symbols, data from Guinier photographs, solid symbols, from the Rietveld refinement.

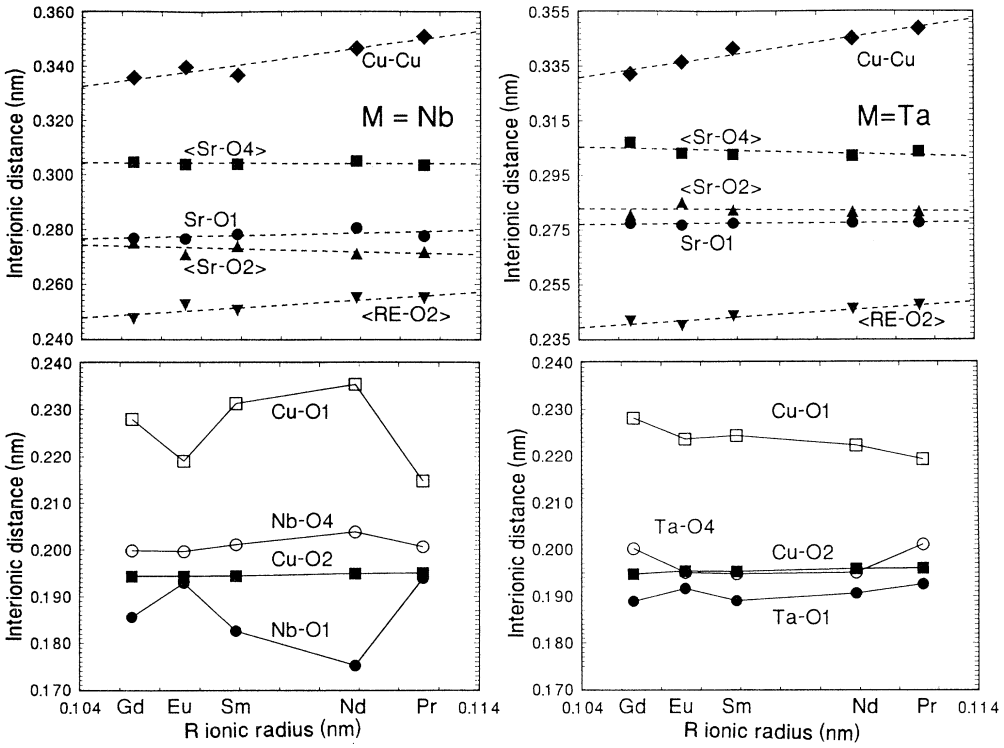

FIG. 7. Interionic distances vs rare-earth ionic radius of R^{3+} (CN=8) in $Sr_2RMCu_2O_{8-\delta}$. Values in brackets are average distances.

tem and by 5.6% for the Ta system, parameter c variations are much smaller, 0.4% and 0.5%, respectively (see Table IV), leading to an overall volume compression for both systems of only about 1.6%.

Figure 7 reveals details of the scaling of the interionic distances with the ionic radii R^{3+}(CN=8) (Ref. 8) in comparison with the lattice contraction. Since rare-earth ions are situated between CuO_2 planes, a change of rare-earth ion mostly affects the nearest neighboring Cu and O(2) ions, but leaves Sr, M, O(1), and O(4) ions nearly untouched. Indeed, all Sr-oxygen distances stay almost constant throughout the rare-earth series studied. The Cu-Cu distance which shows the separation of the CuO_2 planes reveals the most pronounced changes in the system. Its contraction is found to be 1.5 and 1.4 times higher (in absolute values, 0.015 nm and 0.017 nm) than that of the c parameter (0.010 nm and 0.012 nm) and about 3 times higher than the volume contraction (in relative values, 4.2% and 4.8%) for the Nb and Ta systems, respectively.

The relative compression of the average R-O(2) bond length was found to be 3.0% and 2.3% for Nb and Ta systems, respectively, which is also larger than the overall volume compression (1.6% for both systems).

The distance Cu-O(2) is constant for the whole series of the compounds studied, revealing rather stable copper-oxygen bonding within the base of the Cu[O(1),$O(2)_4$] pyramid.

The oxygen ion O(1) was interestingly found to move against the overall lattice contraction towards the M site in such a way, that the Cu-O(1) bond distance expands roughly twice as much as the M-O(1) bond shrinks.

The so-called "puckering" angle, i.e., the angle Cu-O(2)-Cu, was found to be almost constant for both Nb and Ta systems; however, its values (about 174° and 167°, respectively) are larger than the usually observed value of 165° for the related $RBa_2Cu_3O_7$ system, where an empirical value of approximately 167° was found to be critical in respect to the disappearance of superconductivity.[15,16]

3. *Metal substitutions*

Attempts to introduce bulk superconductivity into the 2112 phases by various metals were unsuccessful for the combinations $SrCaRNbCu_2O_8$, R = La, Gd, $Ba_2(La_{1-x}Ca_x)NbCu_2O_8$, and $Sr_2(R_{1-x}Ca_x)NbCu_2O_8$, R = Pr, Sm.

Similarly the samples with nominal compositions $Sr_2RTCu_2O_8$, R = La, Pr and T = Ti, Zr, Mo were all multiphase. In the case of Nb(Ta)/W substitution a small solubility has been observed, rendering single-phase products according to x-ray analysis up to $Ba_2LaNb_{\sim 0.7}W_{\sim 0.3}Cu_2O_8$ and $Ba_2LaTa_{\sim 0.8}W_{\sim 0.2}Cu_2O_8$ after heat treatment under air or oxygen for 75 h at 1000 °C. Traces of superconductivity (with $T_c \sim 30$ K and a variable volume fraction of about 0.2% or less, depending upon the oxygen content) concomitant with a considerable decrease of the room-

temperature resistivity by roughly two orders of magnitude were observed in the latter compounds when a final heat treatment under oxygen was added after treatment in air at 1000 °C. However, we neither succeeded to increase the superconducting volume fraction nor resolved the structure of the superconducting impurity phase.

4. Stability

Previous investigations of the oxygen content in samples of the 2112 system revealed, on the one hand, that the oxygen content is close to the stoichiometric value of 8 (Refs. 3, 4, 17) and on the other hand a higher thermodynamic stability with respect to reduction under a H_2/N_2 gas mixture in differential thermal analysis (DTA) thermogravimetric analysis (TGA) experiments in comparison with the parent 123 system. This was attributed to the presence of Nb(Ta) ions in the structure which are considered to be more stable against reduction than Cu. As the 2112 system was therefore supposed to be rather stable and no further results on its stability over long periods of time under normal laboratory conditions were reported until now, we have repeated a series of measurements on the samples with nominal composition $Sr_2RTaCu_2O_8$ (R = Nd, Sm, Eu) after storage for more than 1 year under normal laboratory conditions (i.e., without any special protection from moist air, etc.). Three sets of measurements were performed for each of the samples treated as follows: a freshly synthesized (as described above) sample, in the following referred to as sample A; a sample after 13-month storage under normal laboratory conditions in form of a powder, sample B; sample B newly pressed and annealed under oxygen at 1030 °C for 24 h and slowly cooled (1 °C/min) to room temperature, sample C.

The results of these investigations can be summarized as follows.

The lattice parameters of samples A and C are practically within their experimental error. On the contrary, both a and c lattice parameters of sample B are larger, showing a small overall lattice expansion of about 0.1%, which could be attributed to oxygen loss of the sample over the long period of storage. The oxygen "recovering" effect observed after appropriate heat treatment could explain the good correspondence of the lattice parameters for samples A and C.

The comparison of Rietveld refinement results for samples A and B show that along with the lattice expansion, the occupancies of two oxygen sites were found to be reduced for sample B: the one for O(1) was found to be 0.94 and the one for O(4), 0.93. On the basis of the obtained oxygen site occupancies we estimate the relative oxygen content for sample B to be about 5% less than that for sample A.

Comparing the average metal-oxygen bond distances and interbond angles we found all of them to stay almost identical for both the A and B samples with two noticeable exceptions: First, the oxygen at the O(1) position in sample B was found to be shifted in the direction to Cu, so that the Ta-O(1) bond enlarges and the

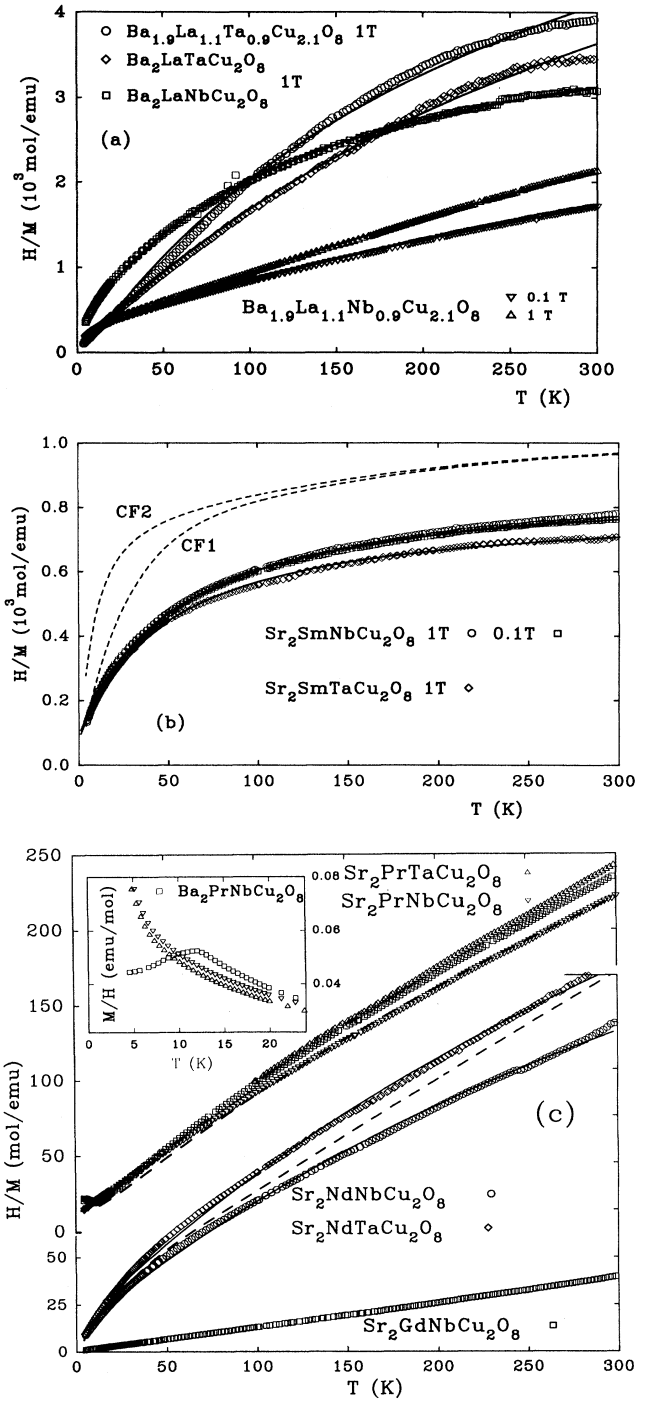

FIG. 8. Inverse susceptibility (H/M at 1 T) as a function of temperature; solid lines are the fit to the modified Curie-Wess law: (a) stoichiometric and off-stoichiometric $Ba_2LaMCu_2O_{8-\delta}$ (M = Nb, Ta) compounds as labeled; (b) $Sr_2SmMCu_2O_{8-\delta}$ (M = Nb, Ta) dashed lines are calculated susceptibilities using CF parameters of $NdBa_2Cu_3O_7$ (Ref. 22) and $PrBa_2Cu_3O_7$ (Ref. 20) labeled as CF1 and CF2, respectively; (c) $Sr_2RMCu_2O_{8-\delta}$ (R = Pr, Nd and M = Nb, Ta) and $Sr_2GdNbCu_2O_{8-\delta}$; dashed lines are calculated susceptibilities using CF parameters of $PrBa_2Cu_3O_7$ (Ref. 20) for $Sr_2PrMCu_2O_{8-\delta}$ and the CF parameters of $NdBa_2Cu_3O_7$ (Ref. 22) for $Sr_2NdMCu_2O_{8-\delta}$.

Cu-O(1) bond shrinks, and second, the tilting angle of the Ta[$O(1)_2, O(4)_4$] octahedra was found to be 2 times smaller for sample B than that for sample A.

B. Magnetic characterization

Shown in Figs. 8(a)–8(c) is the inverse susceptibility of $Sr_2RMCu_2O_8$ (R = Nd, Pr, Sm, Gd; M = Nb, Ta) together with $Ba_2LaMCu_2O_8$. With the exception of $Sr_2EuMCu_2O_8$ the susceptibility data can be fitted with a modified Curie-Weiss (CW) law $\chi = \chi_0 + C/(T - \Theta)$; the results of the temperature-independent susceptibility χ_0, the paramagnetic Curie temperature Θ, and the effective moment μ_{eff} derived from the Curie constant C are collected in Table V. We used the 1-T data for the determination of μ_{eff}, χ_0, and Θ since the high-temperature tail of $\chi(T)$ is slightly field dependent at lower fields but saturates at about 1 T which might arise from antiferromagnetic contributions of the Cu sublattice and/or from magnetic impurities. As an example, $\chi(T)^{-1}$ of $Ba_2LaNbCu_2O_8$ and $Sr_2SmNbCu_2O_8$ at 0.1 and 1 T is displayed in Figs. 8(a) and 8(b). While the 1 T data yield a 40% lower χ_0 than the corresponding 0.1 T measurements, the effective moments remain nearly unaffected.

TABLE V. Magnetic parameters determined from the modified Curie-Weiss fit in the temperature regime 4.2–300 K.

	μ_{eff} (μ_B)	$\chi_0 10^{-3}$ (emu/mol)	θ (K)	T_N (K)
$Ba_2LaNbCu_2O_8$	0.48	0.225	−8.8	
	0.3[a]	0.123[a]	−4.3[a]	
$Ba_{1.9}La_{1.1}Nb_{0.9}Cu_{1.9}O_8$	0.99	0.085	−26	
$Ba_2LaTaCu_2O_8$	0.62	0.125	−1	
$Ba_{1.9}La_{1.1}Ta_{0.9}Cu_{1.9}O_8$	0.53	0.125	3.8	
$Ba_2PrNbCu_2O_8$	2.98	0.88	−10.6	12
$Sr_2PrNbCu_2O_8$	3.02	0.87	−12.8	2.3
	2.95[b]	0.7[b]	−18[b]	< 6[b]
$Sr_2PrTaCu_2O_8$	2.89	0.91	−12	2.2
$Sr_2NdNbCu_2O_8$	3.1	2.02	−13	< 1.7
	3.42[b]	0.4[b]	−45[b]	
$Sr_2NdTaCu_2O_8$	2.87	1.61	−14	< 1.7
$Sr_2SmNbCu_2O_8$	0.68	1.13	−5.8	< 1.5
$Sr_2SmTaCu_2O_8$	0.66	1.22	−5	< 1.5
$Sr_2EuNbCu_2O_8$	0.44	0.99	−5.8	V.V.[c]
$Sr_2EuTaCu_2O_8$	0.43	1.03	−7,12	V.V.[c]
$Sr_2GdNbCu_2O_8$	7.97	0.1	−3.6	2.18
	7.97[b]	0.3[b]	−3[b]	2.15[b]
$Sr_2GdTaCu_2O_8$	8.03	0.1	−2.8	2.18

[a]Bennahamiahs *et al.*, Ref. 17.
[b]Jhans *et al.*, Ref. 14.
[c]Van Vleck susceptibility with λ = 430 K and λ = 425 K (see text) for the Nb and Ta samples, respectively.

1. $Ba_2LaMCu_2O_8$ (M = Nb, Ta)

Because $Sr_2LaMCu_2O_8$ compounds appeared to be multiphase, we use the corresponding Ba compounds in Fig. 8(a) as a reference for the background susceptibility of the Cu-M-O (M = Nb,Ta) sublattice. According to the larger core diamagnetism of Ta in comparison to Nb one expects a larger χ_0 for the latter, which is only observed for the stoichiometric Nb compounds (see Table V). This is also reflected in the larger reciprocal susceptibilities of the Ta compounds in the high-temperature regime with respect to the corresponding Nb compounds. Unresolved remains the nearly 2 times larger μ_{eff} value of the nonstoichiometric $Ba_{1.9}La_{1.1}Nb_{0.9}Cu_{2.1}O_8$ sample although in the stoichiometric samples secondary phases of about 3–8 % have been detected by x-ray analysis. Note that Cu antiferromagnetism has been observed by neutron diffraction in $Ba_2RNbCu_2O_8$ (R = Pr, Nd) below 375 and 340 K, respectively,[13] and in $Sr_2PrTaCu_2O_8$ with a significantly reduced T_N^{Cu} = 190 K (see Sec. III A 1). By analogy with these findings we presume that Cu antiferromagnetism occurs also in these La systems which may modify the high-temperature behavior of the susceptibility causing deviations from the simple modified CW law in Fig. 8(a).

2. $Sr_2RMCu_2O_8$ (R = Pr, Nd, Sm; M = Nb, Ta)

The pronounced curvature of the reciprocal susceptibility of both $Sr_2SmMCu_2O_8$ compounds (M = Nb and Ta) in Fig. 8(b) is described satisfactorily with the modified CW law where χ_0 can be interpreted as the temperature-independent van Vleck susceptibility[18] $\chi_0 = 20N_A\mu_B^2/(7k_B\Delta E)$ due to coupling of the J = 5/2 ground multiplet with the J = 7/2 multiplet separated by an average energy $k_B\Delta E$. From χ_0 we obtain ΔE = 950 and 880 K for the Nb and Ta compounds, which is comparable to Sm_2CuO_4,[19] but smaller than that of the free ion ($\sim$ 1500 K).

We calculated the magnetic susceptibility and specific heat in external fields with the crystal field Hamiltonian in the form of irreducible tensor operators (see, e.g., Ref. 20) and used as a first approximation the crystal field (CF) parameters of the R-123 systems determined from inelastic neutron scattering.[20–22] Despite the structural differences between the R-123 and the R-2112 systems this simple approach is justified since the rare-earth environment is fairly similar in both structures and inelastic neutron data are not yet available for the latter. For Sm-2112 the CF parameters of Nd-123 (Ref. 22) and Pr-123 (Ref. 20) have been used and the calculation including J mixing but without accounting for a possible antiferromagnetic order below 1.5 K yields the susceptibilities [dashed lines in Fig. 8(b)] labeled as "CF1" and "CF2," respectively. In case of the parameters CF1 the second-order CF parameter of Nd-123 (Ref. 22) was modified to obtain the CF splitting for Sm-123O_6 (0,11,32 meV) reported by Guillaume *et al.*[23] The Pr-123 parameters[20] (CF2), without any further modification, yield for the three doublets of the $^6H_{5/2}$ ground multiplet of Sm^{3+}

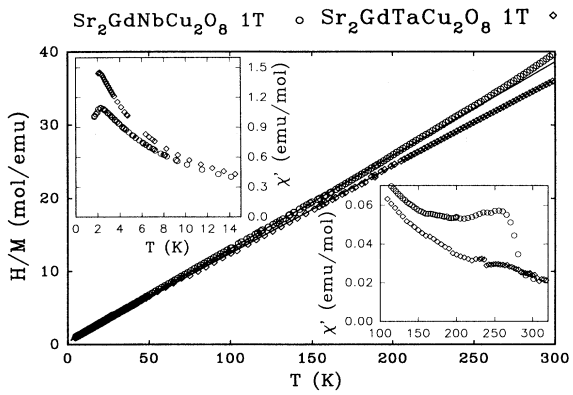

FIG. 9. Inverse susceptibility of $Sr_2GdMCu_2O_{8-\delta}$ (M = Nb,Ta) as a function of temperature; solid line is the fit to the modified CW law, inset: ac susceptibility (80 Hz and 0.1 mT).

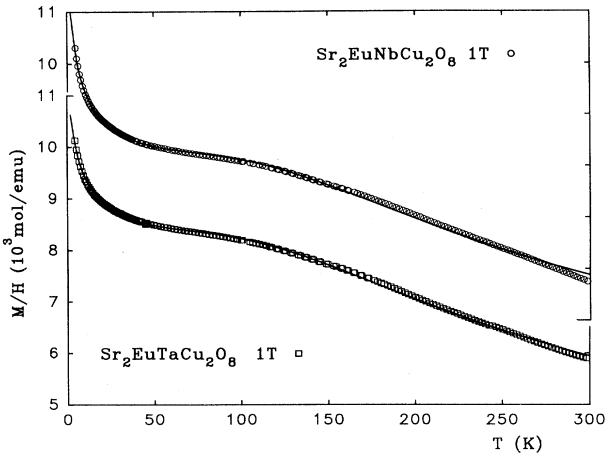

FIG. 10. Susceptibility of $Sr_2EuMCu_2O_{8-\delta}$ (M =Nb,Ta); solid line represents the Van Vleck susceptibility including a Curie-Weiss term; see text.

the level sequence 0, 13.5, 36 meV. As shown in Fig. 8(b) both sets of CF parameters exhibit the characteristic curvature of the inverse susceptibility and differ from one another only in the low-temperature regime. The discrepancy of the absolute susceptibility values between the calculation and the experimental data may arise from a larger calculated separation between the $J = 5/2$ ground multiplet and the $J = 7/2$ multiplet (with an overall splitting between 1500 and 2080 K above the ground state) than the above estimate of ΔE = 880–950 K for the Nb and Ta compounds, respectively, according to the modified Curie-Weiss law.

The inverse susceptibilities of the Pr- and Nd-2112 systems are of the same magnitude and are therefore displayed in Fig. 8(c) separately. Beside the $Sr_2PrMCu_2O_8$ compounds we include in the inset of Fig. 8(c) $Ba_2PrNbCu_2O_8$ which orders antiferromagnetically at 12 K.[9,13] The unexpected reduction of T_N^{Pr} from 12 to 2.3 K across the solid solution $(Ba_{1-x}Sr_x)_2PrNbCu_2O_8$ has been discussed in terms of the hybridization of Pr $4f$ states with the Cu-O valence bands together with an inhomogeneous chemical pressure yielding an anomalous expansion of the Pr-O bond length although the overall volume shrinks upon Ba/Sr substitution; for a further discussion see Ref. 9. The pronounced downturn of the inverse susceptibility at low temperatures of both Nd compounds, indicative for CF contributions, is not properly described by the simple modified CW law. The calculated susceptibilities employing either the CF parameters of Nd-123 according to Goodman *et al.*[21] or Allenspach *et al.*[22] or Pr-123 (Ref. 20) hardly differ from one another for the polycrystalline data (the deviation at room temperature is of the order of the size of the symbols). Shown in Fig. 8(c) are the calculations with the CF parameter set CF2 which provide a satisfactory description of the susceptibility for both the Pr and the Nd compounds and are discussed together with the specific heat data in the next section.

3. $Sr_2RMCu_2O_8$ (R = Eu, Gd; M = Nb, Ta)

Gd-2112 compounds exhibit a rather linear $1/\chi(T)$ [Fig. 8(c)] and small χ_0 due to the vanishing impact of the crystal field upon the $J = S = 7/2$ ground state in contrast to the other R-2112 systems incorporating rare-earth elements with $L \neq 0$. Antiferromagnetic order of the rare-earth sublattice is revealed by a peak in the ac susceptibility (inset, Fig. 9) and the specific heat (see below) for both Gd compounds at 2.18 K which is in agreement with T_N^{Gd} of $Sr_2GdNbCu_2O_8$ determined by Jhans *et al.*[14] The weak but distinct anomaly of the ac susceptibility of $Sr_2GdNbCu_2O_8$ at about 280 K is washed out in higher fields, yielding a shallow deviation from linearity of $1/\chi_{dc}$ versus T which may be attributed to the onset of Cu antiferromagnetism. This feature is not observed for the corresponding Ta compound.

The weakly temperature-dependent susceptibility of the Eu compounds (Fig. 10) being an order of magnitude larger than that of $Ba_2LaNbCu_2O_8$ can be attributed to the Van Vleck susceptibility due to the mixing of the $J = 0$ and $J = 1$ levels plus the thermal population of the higher multiplets given by[18]

$$\chi = N_A \frac{\sum_{J=0}^{6} \left\{ \left[g_J^2 \mu_B^2 J(J+1)/3kT \right] + \alpha_j \right\} (2J+1) e^{-W_J/kT}}{\sum_{J=0}^{6} (2J+1) e^{-W_J/kT}},$$

where $g_J = 3/2$, $W_J = \lambda J(J+1)/2$ are the average energies of the excited J multiplets above $J = 0$, and $\alpha_J = -\mu_B^2/6\lambda$ $(1 \leq J \leq 6)$ and $\alpha_0 = 8\mu_B^2/\lambda$ are the Van Vleck contributions per Eu^{3+} ion. For typical values of the spin-orbit interaction, λ, only terms up to $J = 2$ are significant below room temperature (see also Ref. 19). To account for the background susceptibility of the Cu-Nb-O sublattice we included the modified CW law to this fit of the Van Vleck susceptibility which is represented by the solid line in Fig. 10, yielding the data for μ_{eff}, χ_0, and Θ given in Table V together with $\lambda = 430$ and 425 K for the Nb and Ta compounds, respectively. From Table V the effective moments of the CW term are of the same order as those for $Ba_2LaMCu_2O_8$ and describe the low-temperature upturn of $\chi(T)$ reasonably well.

4. Intercomparison of the effective moments

The results in Table V indicate that μ_{eff} of $Sr_2RNbCu_2O_8$ (R = Pr, Nd, Sm) and the corresponding Ta compounds differ from each other with the tendency that the Nb compounds exhibit slightly larger μ_{eff} values (in particular for Pr, Nd) but with hardly differing χ_0. Even when different temperature regimes are used for the fitting procedure of the modified CW law this feature is preserved, which may be attributed to differences in the Cu antiferromagnetism (AF). On the other hand, considering that χ_0 describes the curvature of $1/\chi(T)$ (i.e., the deviation from the CW law) it incorporates implicitly also the crystal field splitting of the rare-earth ground multiplet and represents in this case an approximation of the Van Vleck susceptibility which reduces the influence of the different core diamagnetism contributions of Nb and Ta visible in the Ba-La systems. Hence the slightly larger μ_{eff} values of the Nb compounds (with the exception of the Gd and Eu system) are not necessarily due to differences in the effective moments of the Cu-M-O sublattice only, since they contain also contributions from the CF splitting. The effective moments of the $Sr_2RMCu_2O_8$ compounds are in between those of fully oxidized and oxygen-depleted $RBa_2Cu_3O_{7-\delta}$ systems but remain below the free R^{3+} values ($\mu_{\text{eff}}^{Pr^{3+}} = 3.58\mu_B$, $\mu_{\text{eff}}^{Nd^{3+}} = 3.62\mu_B$, $\mu_{\text{eff}}^{Sm^{3+}} = 0.845\mu_B$). This together with the reasonable agreement of the calculated susceptibilities using CF parameters of the R-123 compounds indicates that the strength of the CF splitting in the R123 and 2112 systems is similar.

C. Specific heat measurements

A survey of the heat capacity of $Sr_2RMCu_2O_8$ (R= Nd, Sm, Eu and Gd; M = Nb,Ta) (Fig. 11) displays the general low- and high-temperature features of these systems. Besides the clear sign for AF order in the Gd compounds [see inset of Fig. 11(a)] the specific heat anomaly of $Sr_2NdTaCu_2O_8$ which seems to saturate at low temperatures may indicate AF order below 1.7 K. By analogy with the R123 systems and their low ordering temperatures of the R sublattice[24] the low temperature upturns of the heat capacity in $Sr_2NdNbCu_2O_8$ and $Sr_2SmMCu_2O_8$(M = Nb,Ta) also can be regarded as a sign for AF ordering at lower temperatures. Note that AF order of the Nd sublattice has been established by neutron diffraction in $Ba_2NdNbCu_2O_8$ below 1.7 K.[13]

The heat capacity of $Sr_2EuMCu_2O_8$(M = Nb,Ta) [Fig. 11(b)] can be viewed as a representative lattice background specific heat to determine the magnetic and crystal field contributions to C_p for the other rare-earth elements with $J \neq 0$. The low-temperature regime up to 15 K is given by $C_p = \gamma T + \beta T^3 + \delta T^5$ with γ = 3.2 mJ/mol K^2, β = 0.559 mJ/(mol K^4) and $\delta = 9.9 \times 10^{-5}$ mJ/(mol K^4) where β yields the low-temperature limit of the Debye temperature $\Theta_D^{LT} = 365$ K. The positive deviation from the fit below 2.5 K cannot properly be described with an A/T^2 term and may arise from magnetic impurities which cause the low-temperature upturn of the susceptibility in Fig. 10. For the temperature range 4 K $< T <$ 100 K we use a combination of a Debye and four Einstein functions where the characteristic temper-

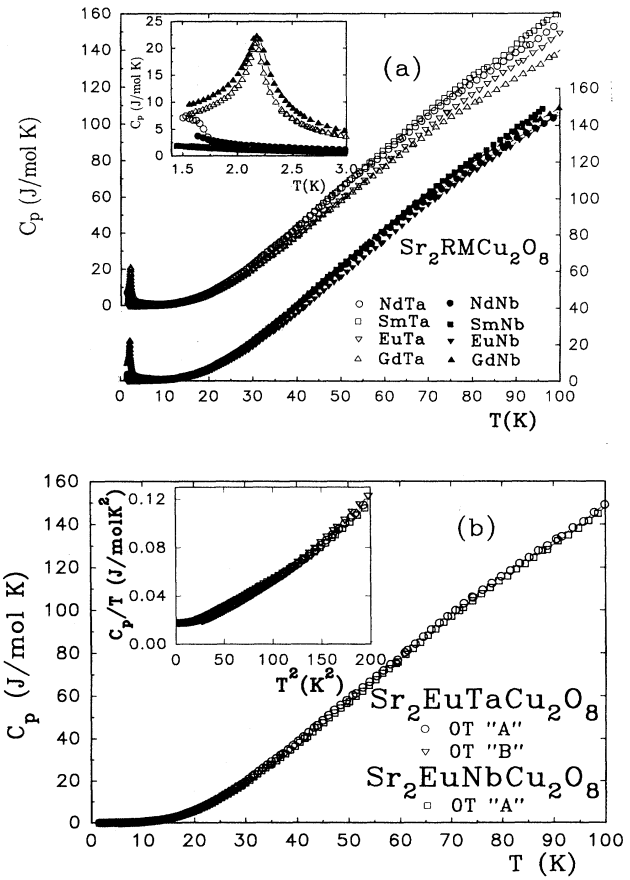

FIG. 11. Specific heat (C_p) of $Sr_2RMCu_2O_{8-\delta}$ (R = Nd, Sm, Eu, Gd, and M = Nb, Ta) as a function of temperature: (a) specific heat of $Sr_2EuMCu_2O_{8-\delta}$ (M =Nb,Ta); inset, C_p/T versus T plot of the low-temperature regime. (b) The labels A and B refer to freshly synthesized samples and after 13 months storage under laboratory conditions, respectively (see Sec. III A 4).

atures Θ_D = 160 K, 167 K; Θ_E^1 = 585 K, 570 K{18}; Θ_E^2 = 302 K, 306 K {11}; Θ_E^3 = 183 K, 174 K{9}; Θ_E^4 = 95 K, 90 K {1} correspond to the 3 acoustic and 39 optical modes for the Nb and Ta compounds, respectively (the number of optical branches for the latter four Einstein temperatures are given in brackets).

To check the influence of the long-term aging upon the lattice specific heat we repeated C_p measurements after 13 months storage of samples under normal laboratory conditions. Although small changes of the lattice parameters together with a reduction of the tilting angle of the Ta[$O(1)_2$,$O(4)_4$] octahedra have been observed, the heat capacity of $Sr_2EuTaCu_2O_8$ remains within the experimental resolution the same [see Fig. 11(b)]. This indicates that aging has no effect upon the lattice specific heat while small changes of $C_p(T)$ in the intermediate-temperature range of the corresponding Sm compounds may be attributed to crystal field effects.

1. $Sr_2GdMCu_2O_{8-\delta}$ (M =Nb, Ta)

A comparison of the specific heat anomalies at T_N of Gd-123O_6/O_7 and $GdBaSrCu_3O_6/O_7$ (Ref. 25) with $Sr_2GdMCu_2O_{8-\delta}$ in Fig. 12 reveals that Ba/Sr substitution in Gd-123 systems yields an analogous broadening of the λ anomaly as the replacement of the Cu-O chains by Nb or Ta-O octahedra. The main difference of the $Sr_2GdMCu_2O_{8-\delta}$ compounds is the shift of T_N^{Gd} to lower temperatures with respect to the Gd-123 systems. No distinct effect between Nb and Ta upon T_N^{Gd} is observed.

To determine the entropy associated with the AF order (which is expected to be Rln8) external fields up to 11 T were applied. The small anomaly at 6.9 K in Fig. 13 is due to a small fraction (~2%) of Gd_2CuO_4 exhibiting at this temperature a sharp λ anomaly due to AF order.[26] As in the Gd-123 systems[25] the AF order is suppressed with an external field and a Schottky anomaly occurs due to the Zeeman splitting of the J = 7/2 ground multiplet which is shifted to higher temperatures with rising external fields. For the calculation of the Schottky anomaly shown as the solid line Fig. 13 we assumed an equidistant splitting of the J = 7/2 multiplet and used the external field as the only free parameter to adjust the position of the maximum of the calculated Schottky anomaly to the experimental maximum in the C_p/T vs T plot with respect to temperature. The Gd contribution to the heat capacity $\Delta C_p(T,H)$, obtained by subtracting $C_p(T)$ of $Sr_2EuNbCu_2O_8$ from the raw data, is in reasonable agreement with the calculated effect of the applied field when we use 4.7, 7.2, and 9.8 T instead of the applied field of 6, 9, and 11 T. The apparent reduction of the external field of about 1.4 T is of the same order as observed for the Gd-123 systems[25] (1.3 T) and seems to be systematic in these systems; its origin, however, remains to be resolved. The deviation between the calculation and the experimental data for 9 and 11 T above 10 K indicates that the lattice contribution of the Gd-Nb sample is underestimated by that of the $Sr_2EuNbCu_2O_2$ compound. Accordingly the entropy gain is slightly growing with the temperature up to 80 K and exceeds the expected value of Rln8 above 50 K for the 9- and 11-T measurements.

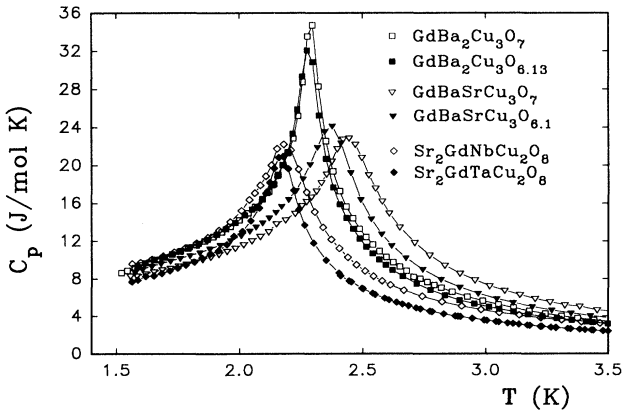

FIG. 12. Comparison of the low-temperature heat capacity of $GdBa_2Cu_3O_7/O_6$, $GdBaSrCu_3O_7/O_6$ (Ref. 25) and $Sr_2GdMCu_2O_{8-\delta}$ (M =Nb,Ta).

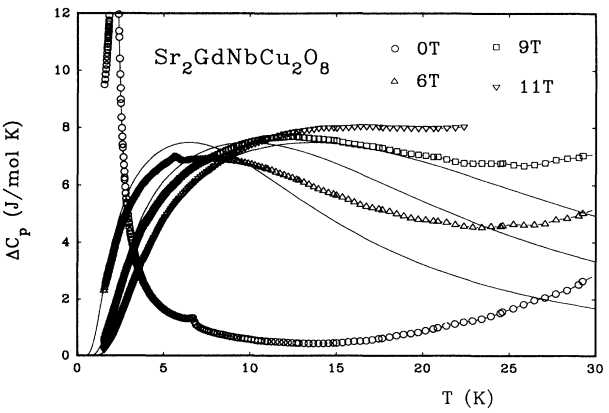

FIG. 13. Gd contribution to the specific heat (ΔC_p) of $Sr_2GdNbCu_2$ $O_{8-\delta}$ for various external fields, solid lines calculated $C_p(T,H)$ including the Zeeman splitting of the external field but without the accounting for the AF order (see text).

2. $Sr_2RMCu_2O_2$ (R=Pr, Nd, Sm; M =Nb, Ta)

For a detailed specific heat study of $Ba_{2-x}Sr_xPrNbCu_2O_8$ we refer to Ref. 9 where the unexpected reduction of T_N from 12 to 2.3 K in this series was discussed in terms of an inhomogeneous volume compression accompanied by an expansion of the Pr-O bond length of about 3.8% which reduces the Pr 4f hybridization with Cu-O valence bands and thus T_N of the Pr sublattice. The same behavior is observed for the corresponding Ta compounds (Fig. 14). As Pr is the only element forming all four 2112 compounds (with Ba,

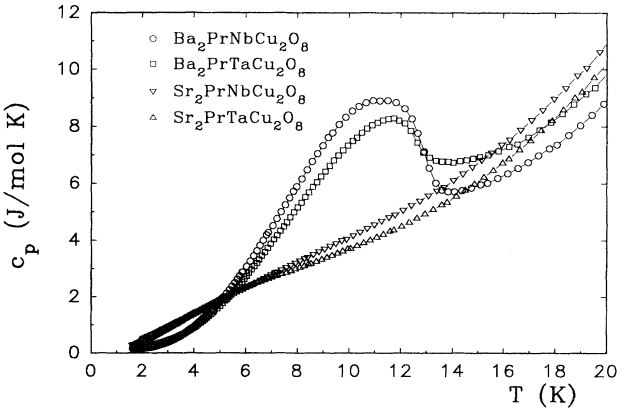

FIG. 14. Specific heat of $Sr_2PrMCu_2O_{8-\delta}$ and $Ba_2PrMCu_2O_{8-\delta}$ as a function of temperature.

Sr, Nb, and Ta; see also Table I) and the AF order of the $Ba_2PrTaCu_2O_8$ is well within the measuring regime we present a comparison of those in Fig. 14. Despite the rather sensitive behavior of the exceptionally high Pr antiferromagnetic order in $PrBa_2Cu_3O_{7-\delta}$ (17 K) upon doping and/or local structural changes [as, e.g., oxygen depletion,[20] hydrogen absorption,[25,27] Cu/3*d* metal,[28] and Ba/Sr (Ref. 25) substitutions], Fig. 14 shows no significant effect between Nb and Ta upon the low-temperature specific heat anomaly associated with T_N^{Pr}. This agrees with the finding for the Gd-2112 system and also for the following Nd- and Sm-2112 compounds. Minor changes of the pronounced C_p anomaly at 12 K between $Ba_2PrNbCu_2O_8$ and $Ba_2PrTaCu_2O_8$ are of the same order as those observed for a variation of the stoichiometry in $Ba_{2-y}Pr_{1+y}Nb_{1-y}Cu_{2+y}O_8$.[9]

The Nd contribution to the heat capacity (ΔC_p) after subtracting the phonon contribution, represented by C_p of the corresponding $Sr_2EuMCu_2O_8$, is displayed together with the calculated heat capacity for various external fields in Figs. 15(a) and 15(b). As for the susceptibility calculation we use the CF parameters of Nd-123 determined from inelastic neutron scattering by Allenspach *et al.*[22] which yield, without accounting for the low-temperature antiferromagnetic order, the splitting of the $^4I_{9/2}$ ground multiplet into five doublets with the following level scheme sequence: 0-12-20-35-116 meV. Although Nd-123O_7 is orthorhombic, the CF levels shift only a little to lower energies upon oxygen depletion for tetragonal Nd-123$O_{7-\delta}$ ($\delta \approx 0.6$ and 1).[22,29] This together with the agreement of the experimental and calculated data (which is the average mean value of C_p with respect to the external field along the *a*, *b*, and *c* directions) in Fig. 15 indicates that the assumption for the CF parameters appears to be a reasonable approach for the *R*-2112 compounds and allows the following interpretation of the C_p data in external fields: A field of 3 T shifts the AF order (at about 1.7 K at zero field) to lower temperatures while a Schottky anomaly due to the Zeeman splitting of the ground state doublet occurs which moves to higher temperatures with growing fields as expected. From the entropy associated with the Schottky anomaly attaining $R\ln 2 = 5.76$ J/(mol K) between 6 and 9 T we conclude that a field as low as 6–9 T is sufficient to suppress the AF order of the Nd sublattice. The second Schottky anomaly with a broad maximum at about 120 K and a tail extending to above room temperature arises from the population of the next excited states at 12, 20, and 35 meV. The Nd contribution to the heat capacity is slightly larger in case of the Ta analog but the overall shape of the temperature and field dependence of C_p is the same for both compounds. The deviation between the calculation and the experimental data may be attributed to a smaller CF splitting than in Nd-123, although a slight difference in the phonon contribution between the Eu and the corresponding Nd compounds might cause a similar effect.

For the Sm-2112 compounds an analogous temperature and field dependence of C_p is expected as for Nd since, according to inelastic neutron scattering of $SmBa_2Cu_3O_6$,[23] the crystal field splits the $^6H_{5/2}$ ground state multiplet of Sm^{3+} into three doublets separated by 11 meV and 32 meV. For the calculation of the specific

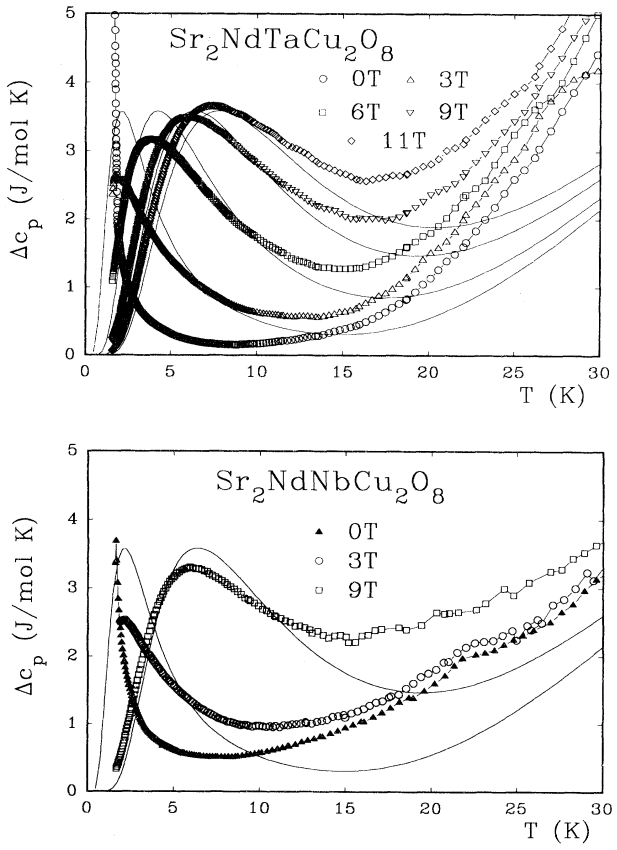

FIG. 15. Nd contribution to the specific heat (ΔC_p) as a function of temperature for various fields, solid line CF calculation with the same CF parameter set [from Nd-123 (Ref. 22)] as that used for the susceptibility.

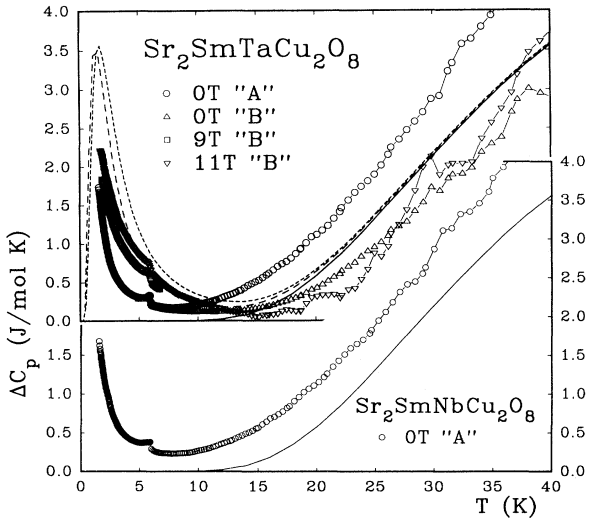

FIG. 16. Sm contribution to the specific heat (ΔC_p) as a function of temperature for various fields, solid, dashed, and dotted lines CF calculations with the CF parameter set CF1 [from Nd-123 (Ref. 22)] for 0, 9, and 11 T. The labels A and B refer to freshly synthesized samples and after 13 month storage under laboratory conditions, respectively (see Sec. III A 4).

heat we use the CF parameters of Nd-123,[22] where the second-order CF parameter (as for the susceptibility) is modified to obtain the second level at 11 meV (CF1). As shown in Fig. 16 the calculated Sm contribution to the specific heat above 20 K (due to the population of the excited levels at 11 and 32 meV) is situated between the measured data of freshly prepared specimens (sample A) and those after a 13 month storage of the samples under normal laboratory conditions (sample B; see also Sec. III A 4). The reduction of ΔC_p between the samples A and B for $T > 10$ K is attributed to the reduction of the CF splitting caused by a smaller tilting angle of the Nb or Ta-O octahedra observed for the aged specimen.

A small fraction of Sm_2CuO_4 as a secondary phase (of about 1–2%) causes the anomaly at 5.95 K which is shifted by 11 T only 140 mK to lower temperatures as previously observed for Sm_2CuO_4.[30] The effect of the external field upon the Zeeman splitting of the ground doublet is for both the calculation and the experimental data significantly smaller for $Sr_2SmTaCu_2O_8$ than in the Nd-2112 systems; compare Figs. 15 and 16. However, it cannot yet be decided whether this arises due to the Ising likeness of the Sm moment in 123 and related systems[31] or due to the symmetry of the ground state because we used the CF parameters of the R-123 compounds as an approximation for those of the R-2112 compounds.

IV. CONCLUSION

An internally consistent set of structural parameters is obtained for the compounds $Sr_2RMCu_2O_{8-\delta}$ with R = Pr, Nd, Sm, Eu, Gd and M = Nb, Ta.

Traces of superconductivity (of the order of less than 0.2%) have been observed in $Ba_2LaM_{1-x}W_xCu_2O_{8-\delta}$ ($x \sim 0.3, M$ = Nb,Ta) below 30 K; however, the superconducting impurity phase could not be identified.

From magnetic and specific heat measurements the overall strength of the crystal field splitting in these R-2112 compounds is similar to that in the corresponding R-123 systems. Antiferromagnetic order of the rare-earth sublattice occurs for both Gd-2112 compounds at 2.18 K and for $Sr_2PrMCu_2O_{8-\delta}$ (M = Nb,Ta) at about 2.3 K, while T_N^R for the Nd and Sm compounds are presumably below 1.8 K. In contrast to the pronounced effect of the isoelectronic Ba/Sr substitution upon the suppression of the Pr antiferromagnetism in $(Ba_{1-x}Sr_x)_2PrNbCu_2O_{8-\delta}$,[9] the replacement of Nb by Ta is found to have no distinct influence upon the shape and position of the low-temperature specific heat anomalies and, hence, upon the AF order of the rare-earth sublattice.

ACKNOWLEDGMENTS

This research was sponsored by the Austrian National Science Foundation (FWF) under Grant Nos. P7620 and P8169 and by the Kärntner Elektrizitätsgesellschaft (KELAG). The work of M.D. was supported by the Grant Agency of the Czech Republic (Grant No. 202/93/1165). The authors are indebted to Auer Remy, Hamburg for a generous gift of rare-earth oxide materials.

[1] N. Murayama, E. Sudo, K. Kani, A. Tsuzuki, S. Kawakami, M. Awano, and Y. Torii, Jpn. J. Appl. Phys. **27**, L1623 (1988).
[2] M.-J. Rey, Ph. Dehaudt, J. Joubert, and A.W. Hewat, Physica C **167**, 162 (1990).
[3] C. Greaves and P.R. Slater, Physica C **161**, 245 (1989).
[4] A. Ichinose, T. Wada, H. Yamauchi, and S. Takanaga, J. Ceram. Soc. Jpn. **97**, 1053 (1989).
[5] L. Mattheiss, Phys. Rev. B **45**, 2442 (1992).
[6] B. Hellebrand, X.Z. Wang, and P.L. Steger, J. Solid State Chem. **110**, 32 (1994).
[7] N. Brnicevic, I. Basic, P. Planicic, M. Tonkovic, M. Forsthuber, G. Hilscher, T. Holubar, H. Michor, H. Kirchmayr, and G. Schaudy, Appl. Supercond. **1**, 519 (1993).
[8] D. Shannon, Acta Crystallogr. A **32**, 751 (1976).
[9] H. Michor, M. Vybornov, T. Holubar, W. Perthold, G. Schaudy, G. Hilscher, and P. Rogl, Physica C **226**, 1 (1994).
[10] D.B. Wiles and R.A. Young, J. Appl. Crystallogr. **14**, 149 (1981).
[11] J. Schefer, P. Fischer, H. Heer, A. Isacson, M. Koch, and R. Thut, Nucl. Instrum. Methods Phys. Res. A **288**, 477 (1990).
[12] V.F. Sears, in *Methods of Experimental Physics, Neutron Scattering*, edited by R. Celotta and J. Levine (Academic

Press, Orlando, FL, 1988), Vol. 23, Pt. A, p. 521.
[13] N. Rosov, J.W. Lynn, H.B. Radousky, M. Bennahmias, T.J. Goodwin, P. Klavins, and R.N. Shelton, Phys. Rev. B **47**, 15 256 (1993).
[14] H. Jhans, S.K. Malik, and R. Vijayaraghavan, Physica C **215**, 181 (1993).
[15] B. Rupp, E. Pörschke, E. Meuffels, P. Allenspach, and P. Fischer, Phys. Rev. B **40**, 4472 (1989).
[16] M. Guillaume, P. Allenspach, W. Henggeler, J. Mesot, B. Roessli, U. Staub, P. Fischer, A. Furrer, and V. Trounov, J. Phys. C **6**, 7963 (1994).
[17] M. Bennahmias, J.C. O'Brien, H.B. Radousky, T.J. Goodwin, P. Klavins, J.M. Link, C.A. Smith, and R.N. Shelton, Phys. Rev. B **46**, 11 986 (1992).
[18] J.H. Van Vleck, *The Theory of Electric and Magnetic Susceptibilities* (Oxford University Press, London, 1965), p. 245ff.
[19] C.L. Seaman, N.Y. Ayoub, T.J. Bornholm, E.A. Early, S. Ghamaty, B.W. Lee, J.T. Markert, J.J. Neumeier, P.K. Tsai, and M.B. Maple, Physica C **159**, 391 (1989).
[20] G. Hilscher, E. Holland-Moritz, T. Holubar, H.-D. Jostarndt, V. Nekvasil, G. Schaudy, U. Walter, and G. Fillion, Phys. Rev. B **49**, 535 (1994)
[21] G.L. Goodman, C-K. Loong, and L. Soderholm, J. Phys. Condens. Matter. **3**, 49 (1991).
[22] P. Allenspach, J. Mesot, U. Staub, M. Guillaume, A. Furrer, S.-I. You, M.J. Kramer, R.W. McCallum, H. Maletto, H. Blook, H. Matka, R. Osborn, M. Arai, Z. Bowdon, and A.D. Taylor, Z. Phys. B **95**, 301 (1994).
[23] M. Guillaume, A. Furrer, and V. Trounov (unpublished).
[24] J.W. Lynn, *High Temperature Superconductivity* (Springer-Verlag, New York, 1990), p. 268.
[25] G. Hilscher, T. Holubar, G. Schaudy, J. Dumschat, M. Strecker, G. Wortmann, X.Z. Wang, B. Hellebrand, and D. Bäuerle, Physica C **224**, 330 (1994).
[26] T. Holubar, H. Michor, G. Schaudy, G. Hilscher, M. Vybornov, and P. Rogl, Physica B **194-196**, 201 (1994).
[27] J.N. Daou, G. Hilscher, N. Pillmayr, and P. Vajda, in *Superconducting Materials, Physics and Application*, edited by A. Niku-Lari (I.I.T.T., Paris, 1991), p. 275.
[28] H.D. Yang, M.W. Lin, C.K. Chiou, and H.W. Lee, Phys. Rev. B **46**, 1176 (1992).
[29] H. Drössler, H.-D. Jostarndt, J. Harnischmacher, J. Kalenborn, U. Walter, A. Severing, W. Schlabitz, and E. Holland-Moritz (unpublished).
[30] T. Holubar, G. Schaudy, N. Pillmayr, G. Hilscher, M. Divis, and V. Nekvasil, J. Magn. Magn. Mater. **104-107**, 479 (1992).
[31] V. Nekvasil, M. Divis, G. Hilscher, and E. Holland-Moritz, J. Alloys Compounds (to be published).

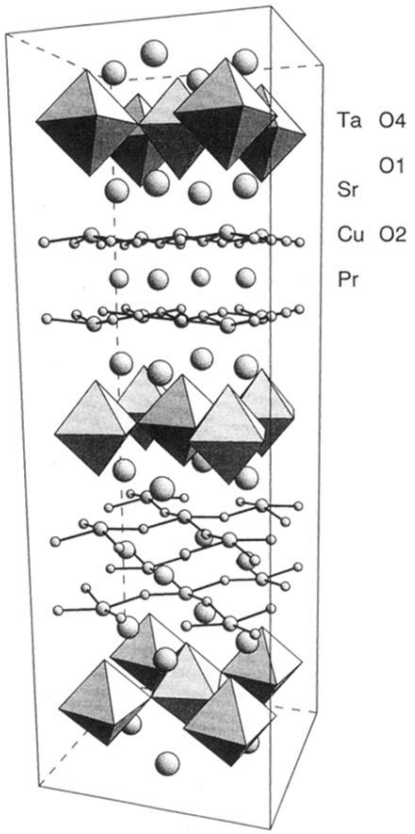

FIG. 1. Crystal structure of $Sr_2PrTaCu_2O_{8-\delta}$ in a three-dimensional perspective view of the CuO_2 planes and TaO_6 octahedra.

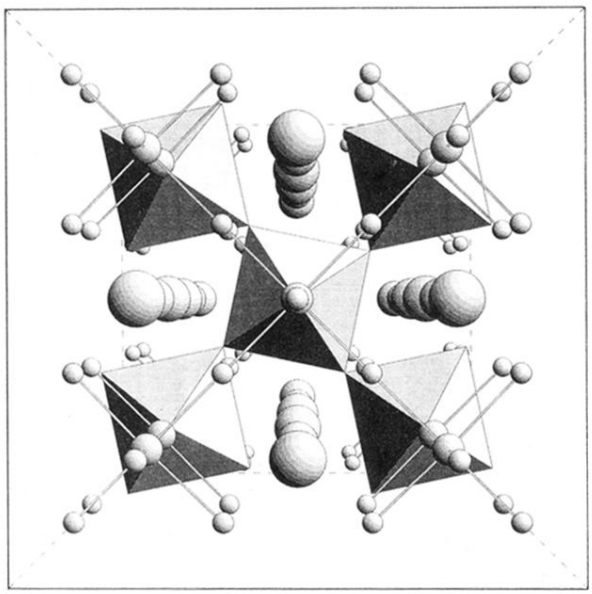

FIG. 2. A view along [001] on the tilting of the corner connected TaO_6 octahedra in $Sr_2PrTaCu_2O_{8-\delta}$.